CONTENTS

C 73 362-1 Furnas Marimbondo System 500kV Substation Design Criteria

C 73 363-9 Design of Detroit Edison SF_6 Compact Substations

C 73 365-4 SF_6 Gas Insulated Stations -- Operation, Rating, Maintenance

C 73 370-4 The Effects of Geomagnetic Storms on Electrical Power Systems

C 73 373-8 Circuit-Breakers in EHV and UHV Networks -- Problems and Solutions

C 73 374-6 Development of a Data Base for Distribution System Planning

C 73 375-3 A Procedure for Calculating the Three Dimensional Electric Field Near a Multiconductor Transmission Line, Including the Effects of the Vertical Ground Wires

C 73 377-9 A Guide for the Selection and Application of Transmission Conductor Stringing Sheaves

C 73 378-7 A Guide to the Conceptual Design of Trnasmission Line Structures IEEE Committee Report

C 73 379-5 Aesthetic Clearing of Transmission Line Right-of-Way

C 73 381-1 Environmental Impact Analysis for Overhead Transmission Lines

C 73 382-9 Quantitative Analysis of Switching Surge Flashover Saturation Characteristics

C 73 383-7 Environmental References for the Design of Electrical Energy Transport Facilities

C 73 384-5 Power Engineering Education for Future Manpower Needs

C 73 386-0 Study of Breakdowns in Vacuum Interrupters

C 73 387-8 The Evolution and Application of Polymers in 5 & 15 KV Switchgear

C 73 388-6 The Effect of Color on Temperature of Electrical Enclosures Subject to Solar Radiation

C 73 390-2 A New TNA -- Part I -- Design Features Provide Versatile Capabilities

C 73 391-0 A New TNA -- Part II -- Capabilities Extend Performance and System Application

C 73 392-8 Dielectric Strength of Laminated Arrangements at 0.1 Hz Voltage

C 73 395-1 Impulse Response of Multiterminal Transformers

C 73 396-9 Dielectric Atress Calculations for EHV Transformer Windings

C 73 397-7 Partial Discharge Tests and Noise Suppression of 500kV Transformers

C 73 398-5 Location of Partial Discharges in Transformers and Reactors from the Measurement of Instantaneous Terminal Voltages at the Instant of Discharge Inception

C 73 401-7 Effects of Tank and Tank Shields on Magentic Fields and Stray Losses in Transformer Windings

C 73 402-5 Harmonics of HV/MV Core-Type Star/Star Distribution Transformers without Auxiliary Delta Winding

C 73 403-3 Magnetization Harmonics in Phase Transformers: Single-Valued BH Representation and Balanced Cores

C 73 404-1 Opitmal Design by Geometric Programming

C 73 405-8 Experience with Modeling EHV Shell-Type Transformers

C 73 408-2 Expression for Switching Impulse Strength Suggesting a Highest Permissible Voltage for A.C. Systems

C 73 409-0 Distortion of Traveling Waves on Three-Phase Transmission Lines

C 73 416-5 Radio Influence Voltage Characteristics of Transmission Line Assemblies Using Semi-Conducting Glazed Insulators

C 73 421-5 Blowing of Distribution Transformer Fuses by Lightning

C 73 422-3 The Application of the Single Equation Econometric Model to Long Range Forecasting for the Public Service Company of New Mexico

C 72 423-1 Means of DC Circuit Breaking in a Three Terminal HVDC System

C 73 424-9 HVDC Convertor Brige: Three Dimensional Chart

C 73 426-4 Digital Simulation of Bipolar HVDC Multiterminal Operation with four Converter Stations and Total Control System

C 73 427-2 Concrete Filled Steel Transmission Poles

C 73 428-0 Finite Element Solution of Wood and Steel Transmission Poles

C 73 429-8 Preliminary Research Studies on Compact Transmission Lines

C 73 431-4 Application of Saturated Reactors to AC Voltage Stabilisation for HVDC Transmission and other Large Convertors

C 73 434-8 Effect of the Dynamic Earth Reflection Coefficient on the Static Wire Surge Impedance

C 73 440-5 Simulating Skin Effects by the Quasi-Frequency Method

C 73 442-1 An Iterative Capacitor Allocation Program for Power Systems (ICAP)

C 73 443-9 Series Capacitors in Power Systems

C 73 444-7 Refraction Coefficient Method for Switching-Surge Calculations on Untransposed Trnasmission Lines (Accurate and Approximate Inclusion of Frequency Dependency)

C 73 446-2 Eddy Current Distribution in Cylindrical Shells of Finite Lenth and Finite Thickness Due to Axial Currents Part I: Current Inside Sheel, Symmetrical Excitation

C 73 447-0 Eddy Cirrent Distribution in Cylindrical Shells of Finite Length and Finite Thickness Due to Axial Currents Part II: Current Inside Shell -- Non Symmetrical Excitation

C 73 448-8 Anomalous Breakdown in Uniform Field Gaps in SF_6

C 73 450-4 Functional Optimization of Hydro-Thermal Systems with Trapezoidal Reservoirs and Variable Efficiency

C 73 452-0 Hydro-Thermal Unit Commitment Using a Dynamic Programming Approach

C 73 454-6 An Efficient Method for the Formation of Bus Impedance Matrix

C 73 455-3 Modification of Z_{bus} Matrix Using Graph Theory

C 73 456-1 Digital Fault Calculations of Large Systems Using Matrix Language and Generalized Equations

C 73 457-9 Application of Bi-Factorisation Techniques for Power System Analysis

C 73 458-7 Optimized Capacitor Allocation Utilizing Generator Compensation Through Z_{bus}

C 73 459-5 System Parameter Dispatching for Generator MVAR Control

C 73 461-1 Optimum Load-Frequency Control of Interconnected Power Systems with Uncertainty

C 73 462-9 Power System Synthesis from Solution of Optimum Transmission loss Coefficients

C 73 464-5 A Non-Linear Block Sor-Newton Load Flow Algorothm

C 73 465-2 Sensitivity Analysis of Load-Flow Solutions

C 73 467-8 A New Development of the Bus Impedance Algorithm

C 73 468-6 A Planning Model for the Analysis of Long-Range Distribution System Design Alternatives

C 73 470-2 Current Limiting Device -- A Utility's Need

C 73 471-0 Regression Analysis of EHV Grid Needs

C 73 474-4 Relative Transient Stability Power Systems Margin Index

C 73 475-1 A Markov Procees Applied to Forecasting Part I: Economic Development

C 73 476-9 Quantitative Evaluation of Permanent Outages in Distribution Systems

C 73 477-7 Reliability Assessment of Transmission and Distribution Schemes

C 73 479-3 Power System State Estimation: Generalizations of the AEP Algorithm with Improved Bad-Data Suppression

C 73 481-9 On-Line Experience with Automatic Generation Control Performance Indices

C 73 483-5 Optimal Power Flow with Complex Variables

C 73 486-8 Output Feedback Control of Power Systems Using a Low Order Model

C 73 488-4 Specific Optimal Control of a Non-Linear Closed-Loop Power System

C 73 489-2 An Output Freedback Proportional-Plus-Integral Regulator for Automatic Generation Control

C 73 490-0 Suboptimal Control of Power Systems with Measurable Output State Variables

C 73 498-3 A study of Treeing in Medium Votage Power Cables

C 73 499-1 Basic Design Characteristics of a Three Conductor Gas-Insulated Power Trnasmission System

C 73 504-8 Diagnostic Testing of Underground Power Cables

C 73 508-9 Power Plant Condenser Cooling System Alternatives in Today's Environment

C 73 509-7 Power Plant Security

C 73 510-5 Low Frequency Rotor Oscillations Introduced by the Excitation System

C 73 511-3 Voltage Regulation Effects of Fast-Acting Speed Governors on Steam Turbine Generators

C 73 512-1 A Thyristorised Chopper Voltage Regulator for Excitation Control of Synchronous Machines

C 73 513-9 Dynamic System Instability for Under-Excited Operation and Effect of Different Loading and Excitation Systems

C 73 514-7 Digital Governor for Use in Computer Control of a Generating Unit

C 73 515-4 Optimal Real and Reactive Power Regulation of a Synchronous Machine

C 73 517-0 Boiler/Turbine Computer Control at Fawley Power Station

C 73 518-8 Closed Loop Digital Automatic Generation Controller

C 73 520-4 Providing Protection Against Electric Shock During Line Construction and Maintenance

C 73 521-2 Impact of Thermal Energy Storage on Power System Planning and Operation

C 73 522-0 Magnetization Harmonics in Phase Transformers:Double-Valued BH Representation and Unbalanced Cores

73 CH0816-9-PWR Transmission Line Failures

CONCEPTS OF DUAL-EXCITED SYNCHRONOUS MACHINE STABILITY AS AFFECTED BY QUADRATURE AXIS EXCITATION CONTROL

M. Goto A. Isono K. Okuda
Hitachi Research Lab., Hitachi Ltd.
Hitachi, Ibaraki, Japan

ABSTRACT

This paper describes the concepts of dual-excited synchronous machine stability as affected by quadrature axis excitation control. A small displacement model of the dual-excited synchronous machine is presented in its general form, in which the two field windings are not necessarily located on the orthogonal axes and may not have the same number of turns nor the same inclination angle to the physical axis of the pole structure. The effect of direct and quadrature axes excitation control was studied on a typical dual-excited synchronous machine with the symmetrical rotor structure, and an excitation control system has been proposed for the dual-excited synchronous machine with two field windings not located on the orthogonal axes. The system offers the same effects on stability as the machine with two field windings located on the orthogonal axes.

INTRODUCTION

The modern electric power system has thrown many difficult problems on stable operation of generators by the increase of long distance transmission lines from remotely located nuclear power stations and of underground cable systems in big cities. The high impedance of the long distance transmission lines is the major problem on transient stability after large disturbances such as a grounding fault and a short circuit fault, have occurred. On the other hand, the generators are often to be operated in the underexcited leading power-factor condition in order to absorb economically the reactive power generated by underground cable systems.

In many papers already published, it has been discussed that the dual-excited synchronous machine shows better characteristics than a conventional machine in both steady state and transient stabilities[1,2]. The idea of the dual-excited synchronous machine was first proposed as a means for improving the transient stability.[3] However, recent studies have shown that this type of machine can also contribute to improve steady state stability limits when it is provided with special control arrangements. Analytical methods on transient and steady state stabilities of this type of machine have been reported[4,5].

This paper describes the contribution of excitation control system including quadrature axis excitation control on steady state stability, and a small displacement model is developed in a general form, with the aid of tensor analysis technique. Then, how the quadrature axis excitation control contributes to improvement of stability, is indicated on a typical dual-excited synchronous machine with the symmetrical rotor structure.

CONFERENCE PAPER

C 73 307-6. A paper recommended by the IEEE Rotating Machinery Committee of the IEEE Power Engineering Society for presentation at the IEEE PES Summer Meeting & EHV/UHV Conference, Vancouver, Can., July 15-20, 1973. Manuscript submitted September 12, 1972; made available for printing April 17, 1973.

Price: Members \$1.35
Nonmembers \$1.80
At Meeting: \$1.00

DYNAMICS OF DUAL-EXCITED SYNCHRONOUS MACHINE CONNECTED TO INFINITE BUS

The dynamics of a dual-excited synchronous machine described in this paper is concerned with excitation control, and such faster phenomena than the excitation control speed as the effects of the rate of change of the armature flux components $p\psi_d$ and $p\psi_q$ and of the amortisseur circuits, are neglected. A power system is considered where a dual-excited synchronous machine having two field windings as indicated in Fig.1 is connected to an infinite bus through an external reactance X_e (See Fig.2). Direct axis (hereinafter called d-axis) in Fig.1 is defined as a direction of the resultant field flux produced by the two field winding f1 and f2. Therefore the quadrature axis (hereinafter called q-axis) excitation component is regarded as zero under a steady state condition. Fig.3 shows a vector diagram of the machine indicated in Fig.2. In this mode, the following equations are obtained.

From the relationship of voltages and currents in Fig.3.

$$e_t^2 = e_d^2 + e_q^2 \tag{1}$$

$$\begin{bmatrix} e_q \\ -e_d \end{bmatrix} = \begin{bmatrix} X_e \end{bmatrix}\begin{bmatrix} i_d \\ i_q \end{bmatrix} + \begin{bmatrix} E\cos\delta \\ -E\sin\delta \end{bmatrix} \tag{2}$$

Under a steady state condition;

$$\begin{bmatrix} e_q \\ -e_d \end{bmatrix} = \begin{bmatrix} \psi_d \\ \psi_q \end{bmatrix} \tag{3}$$

Fluxes in the armature circuit are;

$$\begin{bmatrix} \psi_d \\ \psi_q \end{bmatrix} = -\begin{bmatrix} X_s \end{bmatrix}\begin{bmatrix} i_d \\ i_q \end{bmatrix} + \begin{bmatrix} X_{mf} \end{bmatrix}\begin{bmatrix} i_{f1} \\ i_{f2} \end{bmatrix} \tag{4}$$

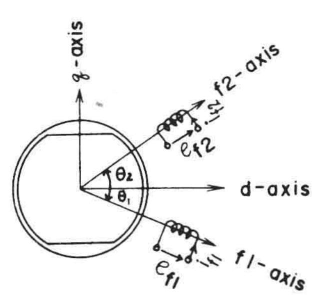

Fig.1. Schematic layout of dual-excited synchronous machine.

From the relationship of voltages and currents in Fig.1;

$$\begin{bmatrix} e_{f1} \\ e_{f2} \end{bmatrix} = \frac{p}{\omega_o}\begin{bmatrix} \psi_{f1} \\ \psi_{f2} \end{bmatrix} + \begin{bmatrix} R_f \end{bmatrix}\begin{bmatrix} i_{f1} \\ i_{f2} \end{bmatrix} \tag{5}$$

Fluxes in the field circuits are;

$$\begin{bmatrix}\psi_{f1}\\ \psi_{f2}\end{bmatrix} = -\left[X_{ma}\right]\begin{bmatrix}i_d\\ i_q\end{bmatrix} + \left[X_r\right]\begin{bmatrix}i_{f1}\\ i_{f2}\end{bmatrix} \tag{6}$$

The torque equation is

$$T_e = \psi_d i_q - \psi_q i_d \tag{7}$$

The equation of motion is

$$Mp^2\delta + Dp\delta + T_e = T_m \tag{8}$$

Next, the quantities in the field circuits expressed in terms of f1 and f2 co-ordinates in Fig.1 are transformed into the quantities expressed in terms of d-axis and q-axis co-ordinates by the transformation matrix (T) as follows.

$$\left[T\right] = \begin{bmatrix}\cos\theta_1 & \cos\theta_2\\ \sin\theta_1 & \sin\theta_2\end{bmatrix} \qquad \theta_1 < 0 \;,\; \theta_2 > 0 \tag{9}$$

$$\begin{bmatrix}i_{fd}\\ i_{fq}\end{bmatrix} = \left[T\right]\begin{bmatrix}i_{f1}\\ i_{f2}\end{bmatrix} \tag{10}$$

$$\begin{bmatrix}\psi_{fd}\\ \psi_{fq}\end{bmatrix} = \left[T\right]_t^{-1}\begin{bmatrix}\psi_{f1}\\ \psi_{f2}\end{bmatrix} \tag{11}$$

$$\begin{bmatrix}e_{fd}\\ e_{fq}\end{bmatrix} = \left[T\right]_t^{-1}\begin{bmatrix}e_{f1}\\ e_{f2}\end{bmatrix} \tag{12}$$

where, $(T)^{-1}$ and $(T)_t$ mean the inverse and transposed matrices respectively. Regarding impedances, the next transformations are executed.

$$\left[X_{MF}\right] = \left[X_{mf}\right]\left[T\right]^{-1} \tag{13}$$

$$\left[X_{MA}\right] = \left[T\right]_t^{-1}\left[X_{ma}\right] \tag{14}$$

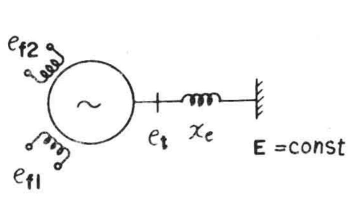

Fig.2. Dual-excited synchronous machine connected to infinite bus through external reactance.

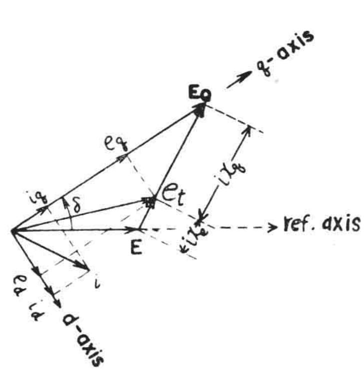

Fig.3. Vector diagram.

$$\left[R_F\right] = \left[T\right]_t^{-1}\left[R_f\right]\left[T\right]^{-1} \tag{15}$$

$$\left[X_R\right] = \left[T\right]_t^{-1}\left[X_r\right]\left[T\right]^{-1} \tag{16}$$

then, eqs. (4), (5) and (6) are converted as follows:

$$\begin{bmatrix}\psi_d\\ \psi_q\end{bmatrix} = -\left[X_s\right]\begin{bmatrix}i_d\\ i_q\end{bmatrix} + \left[X_{MF}\right]\begin{bmatrix}i_{fd}\\ i_{fq}\end{bmatrix} \tag{17}$$

$$\begin{bmatrix}e_{fd}\\ e_{fq}\end{bmatrix} = \frac{p}{\omega_o}\begin{bmatrix}\psi_{fd}\\ \psi_{fq}\end{bmatrix} + \left[R_F\right]\begin{bmatrix}i_{fd}\\ i_{fq}\end{bmatrix} \tag{18}$$

$$\begin{bmatrix}\psi_{fd}\\ \psi_{fq}\end{bmatrix} = -\left[X_{MA}\right]\begin{bmatrix}i_d\\ i_q\end{bmatrix} + \left[X_R\right]\begin{bmatrix}i_{fd}\\ i_{fq}\end{bmatrix} \tag{19}$$

Deriving the relations for a small displacement near the operating point under the linearized approximation from eqs. (1), (2), (3), (7), (8), (17), (18), (19), the following equations are obtained by rearrangement as indicated in appendix.

$$\Delta T_e = \left[K_1\right]\Delta\delta + \left[K_2\right]\begin{bmatrix}\Delta E'_q\\ \Delta E'_d\end{bmatrix} \tag{20}$$

$$\begin{bmatrix}\Delta E'_q\\ \Delta E'_d\end{bmatrix} = \left\{\left[1\right] + \left[T'_{Fd}\right]p\right\}^{-1}\left[K_3\right]\left\{\begin{bmatrix}\Delta E_{fd}\\ \Delta E_{fq}\end{bmatrix} - \left[K_4\right]\Delta\delta\right\} \tag{21}$$

$$\Delta e_t = \left[K_5\right]\Delta\delta + \left[K_6\right]\begin{bmatrix}\Delta E'_q\\ \Delta E'_d\end{bmatrix} \tag{22}$$

The relationship of eqs. (20), (21) and (22) is indicated by the block diagram shown in Fig.4. This block diagram for a small displacement model of the dual-excited synchronous machine is similar to that of the conventional machine, but the coefficients are expressed by matrices.

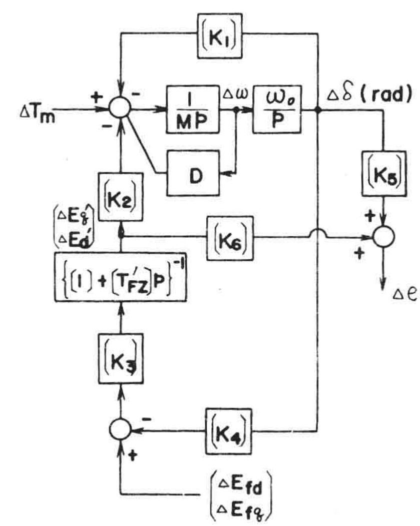

Fig.4. Linearized block diagram of dual-excited synchronous machine connected to infinite bus through external reactance.

Typical Dual-excited Synchronous Machine With Symmetrical Round Rotor

In Fig.1, assuming that the rotor is of the round rotor ($x_q = x_d$) and the two field windings having the same number of turns are symmetrically located against the direct axis as $\theta_1 = -\theta$ and $\theta_2 = \theta$, the reactances and coefficients in Fig.4 become as follows,

$$[X_s] = x_d \begin{bmatrix} 1 & 0 \\ 0 & 1 \end{bmatrix} \tag{23}$$

$$[X_{mf}] = x_{ad} \begin{bmatrix} \cos\theta & \cos\theta \\ -\sin\theta & \sin\theta \end{bmatrix} \tag{24}$$

$$[X_{ma}] = x_{ad} \begin{bmatrix} \cos\theta & -\sin\theta \\ \cos\theta & \sin\theta \end{bmatrix} \tag{25}$$

$$[R_f] = r_f \begin{bmatrix} 1 & 0 \\ 0 & 1 \end{bmatrix} \tag{26}$$

$$[X_r] = x_{ff} \begin{bmatrix} 1 & k\cos 2\theta \\ k\cos 2\theta & 1 \end{bmatrix} \tag{27}$$

$$[T] = \begin{bmatrix} \cos\theta & \cos\theta \\ -\sin\theta & \sin\theta \end{bmatrix} \tag{28}$$

Applying the relations of eqs.(13),(14),(15) and (16) to the above equations;

$$[X_{MF}] = x_{ad} \begin{bmatrix} 1 & 0 \\ 0 & 1 \end{bmatrix} \tag{29}$$

$$[X_{MA}] = X_{ad} \begin{bmatrix} 1 & 0 \\ 0 & 1 \end{bmatrix} \tag{30}$$

$$[R_F] = \frac{2 r_f}{\sin^2 2\theta} \begin{bmatrix} \sin^2\theta & 0 \\ 0 & \cos^2\theta \end{bmatrix} \tag{31}$$

$$[X_R] = \frac{2 x_{ff}}{\sin^2 2\theta} \begin{bmatrix} \sin^2\theta\,(1 + k\cos 2\theta) & 0 \\ 0 & \cos^2\theta\,(1 - k\cos 2\theta) \end{bmatrix} \tag{32}$$

From eq. (A-10) in Appendix the transient reactance is

$$[X_S'] = \begin{bmatrix} x_d' & 0 \\ 0 & x_q' \end{bmatrix} \tag{33}$$

Where,
$$x_d' = x_d - \frac{x_{ad}^2}{x_{ff}} \cdot \frac{2\cos^2\theta}{1 + k\cos 2\theta} \tag{34}$$

$$x_q' = x_q - \frac{x_{ad}^2}{x_{ff}} \cdot \frac{2\sin^2\theta}{1 - k\cos 2\theta} \tag{35}$$

and

$$[C_A]^{-1} = \begin{bmatrix} \dfrac{x_d' + x_e}{x_d + x_e} & 0 \\ 0 & \dfrac{x_q' + x_e}{x_q + x_e} \end{bmatrix} \tag{36}$$

$$[T_{FO}'] = \frac{x_{ff}}{r_f} \begin{bmatrix} 1 + k\cos 2\theta & 0 \\ 0 & 1 - k\cos 2\theta \end{bmatrix}$$

$$\equiv T_{fo}' \begin{bmatrix} 1 + k\cos 2\theta & 0 \\ 0 & 1 - k\cos 2\theta \end{bmatrix} \equiv \begin{bmatrix} T_{fdo}' & 0 \\ 0 & T_{fqo}' \end{bmatrix} \tag{37}$$

$$[K_1] = \left[\frac{E\sin\delta_o}{x_d' + x_e} (e_{do} - x_d' i_{qo}) + \frac{E\cos\delta_o}{x_q' + x_e} (e_{qo} + x_q' i_{do}) \right] \tag{38}$$

$$[K_2] = \begin{bmatrix} \dfrac{E\sin\delta_o}{x_d' + x_e} & \dfrac{E\cos\delta_o}{x_q' + x_e} \end{bmatrix} \equiv \begin{bmatrix} K_{2d} & K_{2q} \end{bmatrix} \tag{39}$$

$$[K_3] = \begin{bmatrix} \dfrac{x_d' + x_e}{x_d + x_e} & 0 \\ 0 & \dfrac{x_q' + x_e}{x_q + x_e} \end{bmatrix} \equiv \begin{bmatrix} K_{3d} & 0 \\ 0 & K_{3q} \end{bmatrix} \tag{40}$$

$$[K_4] = \begin{bmatrix} \dfrac{x_d - x_d'}{x_d' + x_e} E\sin\delta_o \\ \dfrac{x_q - x_q'}{x_q' + x_e} E\cos\delta_o \end{bmatrix} \equiv \begin{bmatrix} K_{4d} \\ K_{4q} \end{bmatrix} \tag{41}$$

$$[K_5] = \left[-\frac{x_d'}{x_d + x_e} \cdot \frac{e_{qo}}{e_{to}} E\sin\delta_o + \frac{x_q'}{x_q + x_e} \cdot \frac{e_{do}}{e_{to}} E\cos\delta_o \right] \tag{42}$$

$$[K_6] = \begin{bmatrix} \dfrac{x_e}{x_d' + x_e} \cdot \dfrac{e_{qo}}{e_{to}} & \dfrac{-x_e}{x_q' + x_e} \cdot \dfrac{e_{do}}{e_{to}} \end{bmatrix} \equiv \begin{bmatrix} K_{6d} & K_{6q} \end{bmatrix} \tag{43}$$

$$\left\{ [1] + [T_{FZ}'] P \right\}^{-1} = \begin{bmatrix} \dfrac{1}{1 + T_{fdz}' P} & 0 \\ 0 & \dfrac{1}{1 + T_{fqz}' P} \end{bmatrix} \tag{44}$$

Though $x_q = x_d$ numerically in the above equations, the individual symbols of reactances are used to keep each original meaning. In this case, the block diagram of the small displacement model is shown in Fig.5, in which the paths indicated by the dotted lines show the loops produced by the q-axis excitation component. It is interesting that the angle θ between a field winding and d-axis affects both the transient reactances and the equivalent field winding time constants.

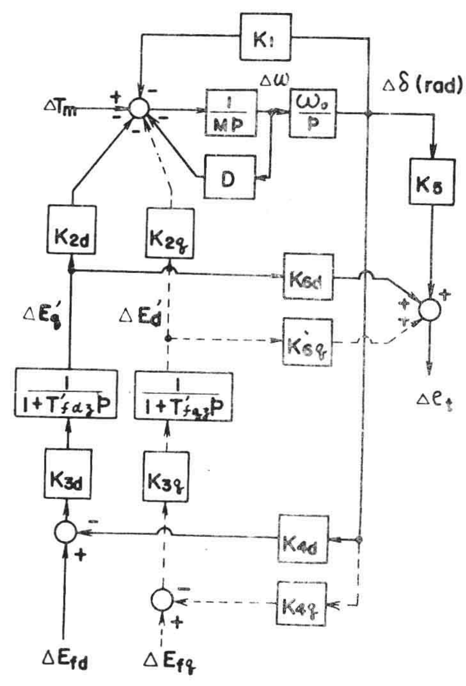

Fig.5. Linearized block diagram of typical dual-excited synchronous machine with symmetrical rotor structure.

Stability of Dual-excited Synchronous Machine

In a dual-excited synchronous machine, it is assumed that the d-axis excitation component is controlled by an automatic voltage regulator (AVR) which functions in response to variation of the generator terminal voltage, and the q-axis excitation component is controlled by an automatic rotor angle regulator (AAR) which functions in response to variation of the rotor angle. Introducing this excitation control system to the block diagram Fig.5, the block diagram Fig.6 is obtained. In Fig.6, $G_{vr}(p)$ and $G_{ar}(p)$ express transfer functions of AVR and AAR respectively.

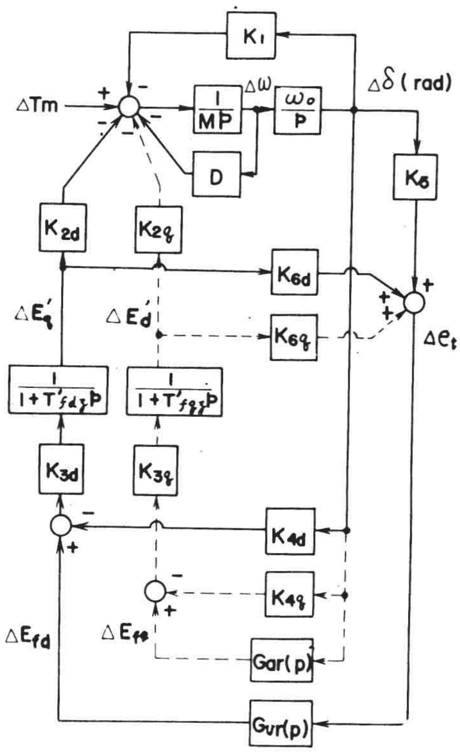

Fig.6. Linearized block diagram of typical dual-excited synchronous machine with AVR and AAR.

The torque components ΔT_d produced by d-axis excitation component and ΔT_q produced by q-axis excitation component are expressed respectively as follows.

$$\Delta T_d = G_d(p)\Delta\delta \tag{45}$$

$$G_d(p) = \frac{K_{2d}K_{3d}}{1+T'_{fdz}p}\left\{\frac{K_{3q}K_{6q}}{1+T'_{fqz}p}\left(G_{ar}(p)-K_{4q}\right)G_{vr}(p)+K_5G_{vr}(p)-K_{4d}\right\}$$
$$\cdot\left\{1-\frac{K_{3d}K_{6d}G_{vr}(p)}{1+T'_{fdz}p}\right\}^{-1} \tag{46}$$

$$\Delta T_q = G_q(p)\Delta\delta \tag{47}$$

$$G_q(p) = \frac{K_{2q}K_{3q}}{1+T'_{fqz}p}\left(G_{ar}(p)-K_{4q}\right) \tag{48}$$

. These torque components are functions of angular frequency ω of the synchronous machine oscillation. Substituting $p=j\omega$ into eq.(20) and decomposing ΔT_d into the real and imaginary parts,

$$\Delta T_d = G_d(j\omega)\Delta\delta$$
$$= \mathrm{Real}\{G_d(j\omega)\}\Delta\delta + j\,\mathrm{Imag}\{G_d(j\omega)\}\Delta\delta \tag{49}$$

where Real{ } =real part, Imag{ } =imaginary part.

Furthermore, substituting the relation $\Delta\delta=\frac{\omega_o}{j\omega}\Delta\omega$ into the above equation, the following equation is obtained.

$$\Delta T_d = \mathrm{Real}\{G_d(j\omega)\}\Delta\delta + \frac{\omega_o}{\omega}\mathrm{Imag}\{G_d(j\omega)\}\Delta\omega \tag{50}$$

In the similar manner on ΔT_q,

$$\Delta T_q = \mathrm{Real}\{G_q(j\omega)\}\Delta\delta + \frac{\omega_o}{\omega}\mathrm{Imag}\{G_q(j\omega)\}\Delta\omega \tag{51}$$

In eqs. (50) and (51), coefficients of $\Delta\delta$ are of the synchronizing torque coefficients and those of $\Delta\omega$ are of the damping torque coefficients.[6]

For the dual-excited synchronous machine being stable, the total synchronizing torque coefficient K_{syn}, the total damping torque coefficient K_{damp}, depending on angular frequency ω of the synchronous machine oscillation, and the steady state total synchronizing torque coefficient K_{syno} for $\omega=0$ in eqs. (52), (53) and (54) have to be positive respectively.

$$K_{syn} = K_1 + \mathrm{Real}\{G_d(j\omega)\} + \mathrm{Real}\{G_q(j\omega)\} \tag{52}$$

$$K_{damp} = D + \frac{\omega_o}{\omega}\mathrm{Imag}\{G_d(j\omega)\} + \frac{\omega_o}{\omega}\mathrm{Imag}\{G_q(j\omega)\} \tag{53}$$

$$K_{syno} = K_1 + G_d(0) + G_q(0) \tag{54}$$

EFFECTS OF QUADRATURE AXIS EXCITATION CONTROL ON STABILITY

Steady State Synchronizing Torque Coeffecient

The torque component ΔT_q produced by q-axis excitation component is indicated in eq.(47). Since q-axis is orthogonal to d-axis, the q-axis excitation component ΔE_{fq} in Fig.6 is zero under a steady state condition. Therefore, the transfer function $G_{ar}(p)$ of AAR in Fig.6 has to satisfy the following equation.

$$G_{ar}(0) = 0 \tag{55}$$

The steady state synchronizing torque coefficient $G_q(0)$ is obtained from eq.(48), under the condition of eq.(55).

$$G_q(0) = K_{2q}K_{3q}\left(G_{ar}(0)-K_{4q}\right) = -K_{2q}K_{3q}K_{4q} \tag{56}$$

It is understood that the q-axis excitation control does not affect the steady state synchronizing torque coefficient. Because of the existence of the q-axis transient reactance x_q', K_1 in the block diagram Fig.6 takes a larger value than that of a conventional machine. However, the demagnetizing effect of the q-axis field flux indicated in eq.(56) acts as a negative feedback component for K_1 and the resultant value is

$$K_1 + G_q(0) = K_1 - K_{2q}K_{3q}K_{4q}$$

$$= \frac{E\sin\delta_o}{x_d' + x_e}(e_{do} - x_d' i_{qo}) + \frac{E\cos\delta_o}{x_q' + x_e}(e_{qo} + x_q' i_{do})$$

$$- \frac{E\cos\delta_o}{x_q' + x_e} \cdot \frac{x_q' + x_e}{x_q + x_e} \cdot \frac{x_q - x_q'}{x_q' + x_e} E\cos\delta_o$$

$$= \frac{E\sin\delta_o}{x_d' + x_e}(e_{do} - x_d' i_{qo}) + \frac{E\cos\delta_o}{x_q + x_e}(e_{qo} + x_q i_{do}) \quad (57)$$

which is the same equation as K_1 of a conventional machine.

Damping Torque Coefficient

The damping torque coefficient is examined when the $G_{ar}(p)$ is indicated in eq.(58) which satisfies the eq.(55).

$$G_{ar}(p) = \frac{K_{ar}\, p}{1 + T_{ar}\, p} \quad (58)$$

The torque component $\triangle T_q$ which is produced by the q-axis excitation is obtained from eqs.(47),(48),(58) as follows;

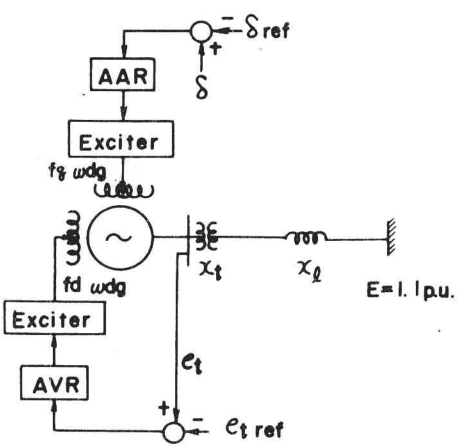

Fig.7. Model system.

Table I Machine and System Constants

Generator and Power System

x_d	= 1.60 (p.u.)
x_q	= 1.60 (")
x_d'	= 0.30 (")
x_q'	= 0.30 (")
T_{fo}'	= 6.0 (sec.)
M	= 7.0 (")
T_{fd}'	= 9.0 (")
T_{fq}'	= 3.0 (")
θ	= 30.0 (deg)
D	= 10.0 (pu Torque/pu speed)
x_t	= 0.15 (p.u.)
x_ℓ	= 0.1 (")

Excitation System

AVR :	$\frac{-100}{1+0.05P}$
AAR :	$\frac{-P}{1+0.05P}$

$$\triangle T_q = \frac{K_{2q} K_{3q}}{1 + T_{fqz}' p}\left(\frac{K_{ar}\, p}{1 + T_{ar}\, p} - K_{4q}\right)\triangle\delta \quad (59)$$

Substituting $p = j\omega$ into eq.(59) and decomposing $\triangle T_q$ into the synchronizing torque component and the damping torque component,

$$\triangle T_q = \left[\frac{\omega^2 K_{2q} K_{3q} K_{ar}(T_{fqz}' + T_{ar})}{\{1+(\omega T_{fqz}')^2\}\{1+(\omega T_{ar})^2\}} - \frac{K_{2q} K_{3q} K_{4q}}{1+(\omega T_{fqz}')^2}\right]\triangle\delta$$

$$+ \left[\frac{\omega_o K_{2q} K_{3q} K_{ar}(1-\omega^2 T_{ar} T_{fqz}')}{\{1+(\omega T_{fqz}')^2\}\{1+(\omega T_{ar})^2\}} + \frac{\omega_o K_{2q} K_{3q} K_{4q} T_{fqz}'}{1+(\omega T_{fqz}')^2}\right]\triangle\omega \quad (60)$$

where the coefficient of $\triangle\omega$ is the damping torque coefficient. The second term of the damping torque coefficient is produced by the demagnetizing effects of the q-axis excitation component and given by

$$\frac{\omega_o K_{2q} K_{3q} K_{4q} T_{fqz}'}{1+(\omega T_{fqz}')^2} = \frac{x_q - x_q'}{x_q + x_e} \cdot \frac{(E\cos\delta_o)^2}{x_q' + x_e} \cdot \frac{\omega_o T_{fqz}'}{1+(\omega T_{fqz}')^2} \quad (61)$$

which always gives positive damping torque. On the other hand, the first term of the damping torque coefficient is produced by AAR and given by

$$\frac{\omega_o K_{2q} K_{3q} K_{ar}(1-\omega^2 T_{ar} T_{fqz}')}{\{1+(\omega T_{fqz}')^2\}\{1+(\omega T_{ar})^2\}}$$

$$= \frac{\omega_o E\cos\delta_o}{x_q + x_e} \cdot \frac{K_{ar}(1-\omega^2 T_{ar} T_{fqz}')}{\{1+(\omega T_{fqz}')^2\}\{1+(\omega T_{ar})^2\}} \quad (62)$$

which is proportional to $\cos\delta_0$. Therefore it diminishes as δ_0 approaches 90 degrees and it goes into negative region when δ_0 exceeds 90 degrees.

This nature is investigated on a model system as shown in Fig.7 where a dual-excited synchronous machine is connected to an infinite bus. Constants used in the calculation are listed up in Table I. Since the study

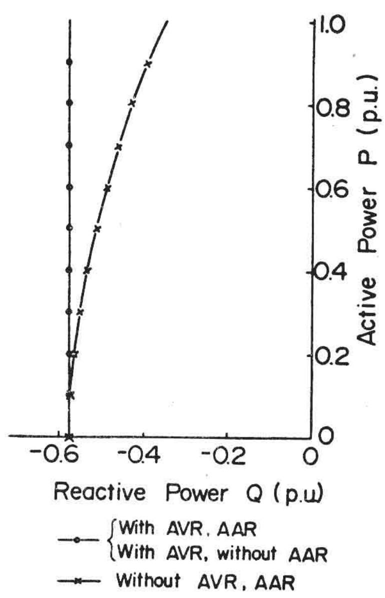

Fig.8. Stability limit curves.

is focused on the effect of the q-axis excitation control, let us assume that AVR and AAR do not directly control the actual field windings f1 and f2 but they control the equivalent field windings fd and fq as indicated in eq.(12). This can be realized by the method discussed in the forthcoming section. The stability limit curves are shown in Fig.8. Various torque coefficients under the operating condition of P=0.9 are shown in Figs.9,10 and 11. These results show that the stable region at P=0.9 is limited at a point where K_{syno} becomes negative. This nature is also seen at lower machine output though the curves are omitted. K_{syno} reverses its sign discontinuously as shown in Fig.9 at an operating point with certain reactive power when the machine is controlled by AVR. Substituting p=0, $G_{ar}(0)=0$ $G_{vr}(0)=-K_{vr}$ (K_{vr} ; AVR gain) in eq.(46),

$$G_d(0)=\frac{K_{2d}\ K_{3d}\ (K_{3q}K_{4q}K_{6q}K_{vr}-K_5K_{vr}-K_{4d})}{1+K_{3d}K_{6d}K_{vr}} \qquad (63)$$

The reactive power output, then the rotor angle increases, K_{6d} becomes smaller and furthermore gets into negative region. Under the above mentioned condition, the value of $(1+K_{3d}K_{6d}K_{vr})$ reaches zero, so K_{syno} reverses its sign discontinuously.

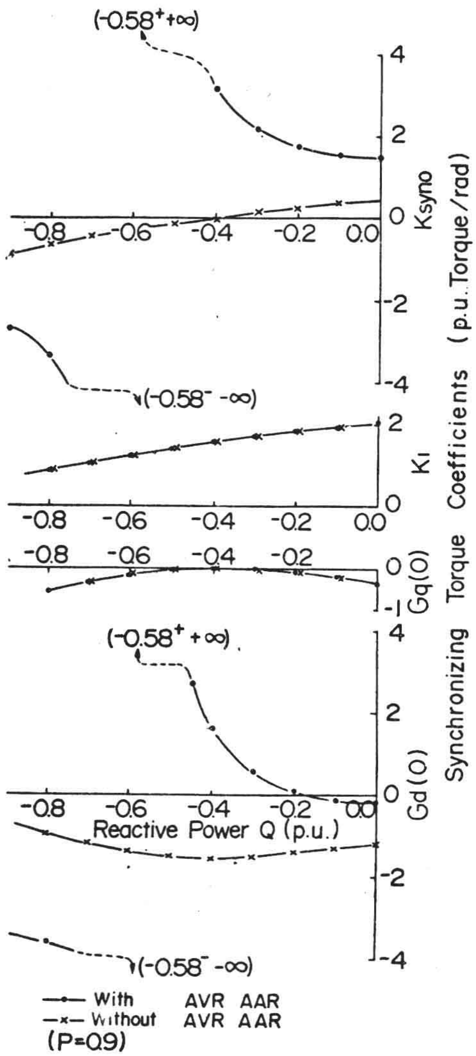

Fig.9. Steady state synchronizing torque coefficients.

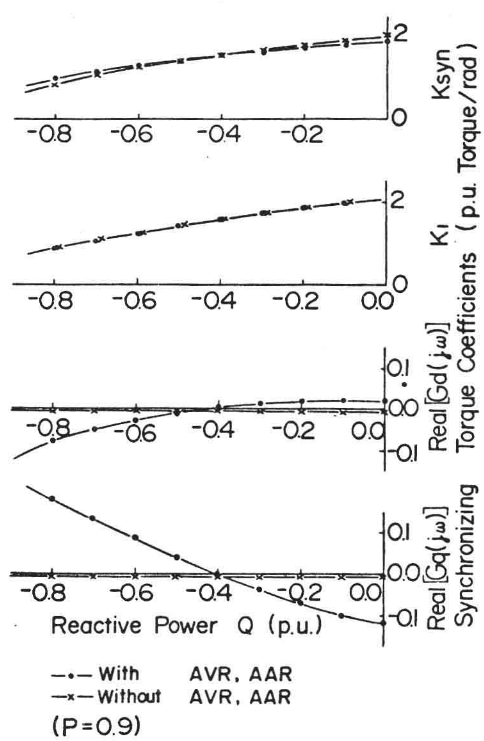

Fig.10. Synchronizing torque coefficients.

In the other case where the impedance of transmission line is larger than that of the model system shown in Fig.7, the stable region may be limited by K_{damp} becoming negative though K_{syno} is positive. The q-axis excitation control is able to increase the value of K_{damp} and is effective for damping oscillation but its effect diminishes when δ approaches 90 degrees. The q-axis excitation control does not greatly contribute to expand the stable region.

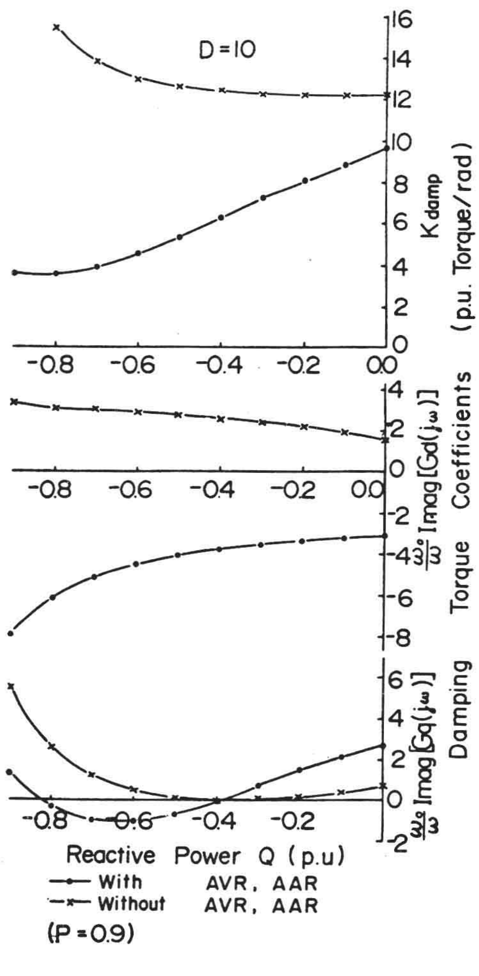

Fig.11. Damping torque coefficients.

EXCITATION CONTROL SYSTEM FOR DUAL-EXCITED SYNCHRONOUS MACHINE

It has been proved that the quadrature axis excitation control increases the synchronous machine damping torque. The next problem is then to find out an optimal control system utilizing this nature. In practice the two field windings f1 and f2 are rarely located on the orthogonal axes. And the both field windings are excited under the steady state condition. Then d-axis or q-axis rarely agrees with the direction of f1-axis or f2-axis. Therefore, if it were so arranged that AVR controlled one of the field windings and AAR the other, AVR would act to vary the d-axis excitation component and partly the q-axis component while AAR would act to vary the q-axis component and partly the d-axis one. And, accordingly, the satisfactory result could not be obtained in this arrangement. To make the control effective as aforementioned, the q-axis excitation components should be controlled by AAR.

Figure 12 shows one of the methods to achieve the expected control in excitation for a typical dual-excited synchronous machine with a symmetrical round rotor. Wherein the output signals of AVR and AAR are fed to the exciter devices for the f1 and f2 windings via the transposed matrix of the transformation matrix eq.(28) and is surrounded by dotted lines in the figure. Through this procedure, AVR can successfully control only the resultant d-axis excitation component produced by the f1 and f2 windings and AAR can do only the resultant q-axis component.

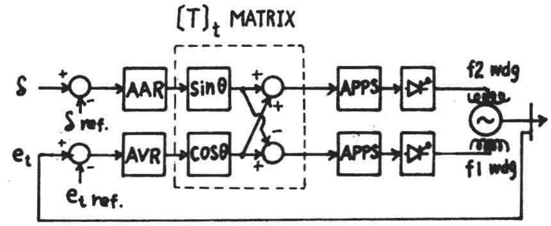

Fig.12. Proposed excitation control system for dual-excited synchronous machine.

CONCLUSION

A small displacement model of a dual-excited synchronous machine was derived by the tensor analysis technique and the contribution of the q-axis excitation control on improving the dual-excited synchronous machine stability was examined by various torque coeffcients produced from the excitation control system. As the results, it has turned out that the q-axis excitation can increase the damping torque coefficient in stable region but it does not greatly contribute to the expansion of stable region. Furthermore, a method to apply the q-axis excitation control system to a dual-excited synchronous machine in which two field windings are not located on the orthogonal axes has been proposed.

ACKNOWLEDGMENT

The authors wish to thank Messrs. M. Nishi, S. Tateishi, E. Shoyama of Hitachi works and Y. Kitano of Kokubu works and Y. Kato of Hitachi Head office for their helpful discussions, and Dr. E. Kobayashi and Dr. T. Maekawa of Hitachi Research Laboratory for their valuable suggestions and encouragement.

APPENDIX

From eqs. (1), (2), (3), (17), (18), (19), (7) and (8), the following equations can be derived by relating the small changes near the operating point under linearized approximation.

$$\Delta e_t = \begin{bmatrix} \dfrac{e_{qo}}{e_{to}} & -\dfrac{e_{do}}{e_{to}} \end{bmatrix} \begin{bmatrix} \Delta e_q \\ -\Delta e_d \end{bmatrix} \equiv [C_{eo}] \begin{bmatrix} \Delta e_q \\ -\Delta e_d \end{bmatrix} \tag{A-1}$$

$$\begin{bmatrix} \Delta e_q \\ -\Delta e_d \end{bmatrix} = [X_e] \begin{bmatrix} \Delta i_d \\ \Delta i_q \end{bmatrix} - \begin{bmatrix} E\sin\delta_o \\ E\cos\delta_o \end{bmatrix} \Delta\delta \tag{A-2}$$

$$\begin{bmatrix} \Delta e_q \\ -\Delta e_d \end{bmatrix} = \begin{bmatrix} \Delta\psi_d \\ \Delta\psi_q \end{bmatrix} \tag{A-3}$$

$$\begin{bmatrix} \Delta\psi_d \\ \Delta\psi_q \end{bmatrix} = -[X_s] \begin{bmatrix} \Delta i_d \\ \Delta i_q \end{bmatrix} + [X_{MF}] \begin{bmatrix} \Delta i_{fd} \\ \Delta i_{fq} \end{bmatrix} \tag{A-4}$$

$$\begin{bmatrix} \Delta e_{fd} \\ \Delta e_{fq} \end{bmatrix} = \frac{p}{\omega_o} \begin{bmatrix} \Delta\psi_{fd} \\ \Delta\psi_{fq} \end{bmatrix} + [R_F] \begin{bmatrix} \Delta i_{fd} \\ \Delta i_{fq} \end{bmatrix} \tag{A-5}$$

$$\begin{bmatrix} \Delta\psi_{fd} \\ \Delta\psi_{fq} \end{bmatrix} = -[X_{MA}] \begin{bmatrix} \Delta i_d \\ \Delta i_q \end{bmatrix} + [X_R] \begin{bmatrix} \Delta i_{fd} \\ \Delta i_{fq} \end{bmatrix} \tag{A-6}$$

$$\Delta T_e = [-\psi_{qo} \;\; \psi_{do}] \begin{bmatrix} \Delta i_d \\ \Delta i_q \end{bmatrix} + [i_{qo} \;\; -i_{do}] \begin{bmatrix} \Delta\psi_d \\ \Delta\psi_q \end{bmatrix}$$

$$\equiv [\psi_o] \begin{bmatrix} \Delta i_d \\ \Delta i_q \end{bmatrix} + [I_o] \begin{bmatrix} \Delta\psi_d \\ \Delta\psi_q \end{bmatrix} \tag{A-7}$$

$$Mp^2\Delta\delta + Dp\Delta\delta + \Delta T_e = \Delta T_m \tag{A-8}$$

Eliminating $(\Delta i_{fd}, \Delta i_{fq})$ from eqs. (A-4) and (A-6)

$$\begin{bmatrix} \Delta\psi_d \\ \Delta\psi_q \end{bmatrix} = -[X_s'] \begin{bmatrix} \Delta i_d \\ \Delta i_q \end{bmatrix} + [X_{MF}][X_R]^{-1} \begin{bmatrix} \Delta\psi_{fd} \\ \Delta\psi_{fq} \end{bmatrix} \tag{A-9}$$

where $$[X_s'] = [X_s] - [X_{MF}][X_R]^{-1}[X_{MA}] \tag{A-10}$$

$(\Delta i_d, \Delta i_q)$ is expressed as follows by eliminating $(\Delta\psi_d, \Delta\psi_q)$ from eqs. (A-2), (A-3) and (A-9).

$$\begin{bmatrix} \Delta i_d \\ \Delta i_q \end{bmatrix} = [X_s' + X_e]^{-1} \left\{ [X_{MF}][X_R]^{-1} \begin{bmatrix} \Delta\psi_{fd} \\ \Delta\psi_{fq} \end{bmatrix} + \begin{bmatrix} E\sin\delta_o \\ E\cos\delta_o \end{bmatrix} \Delta\delta \right\} \tag{A-11}$$

where $$[X_s' + X_e] = [X_s'] + [X_e] \tag{A-12}$$

From eqs. (A-7), (A-9) and (A-11)

$$\Delta T_e = \{[\psi_o] - [I_o][X_s']\}[X_s' + X_e]^{-1} \begin{bmatrix} E\sin\delta_o \\ E\cos\delta_o \end{bmatrix} \Delta\delta + \{[\psi_o] + [I_o][X_s']\}[X_s' + X_e]^{-1} \begin{bmatrix} \Delta E_q' \\ \Delta E_d' \end{bmatrix} \tag{A-13}$$

where $$\begin{bmatrix} \Delta E_q' \\ \Delta E_d' \end{bmatrix} = [X_{MF}][X_R]^{-1} \begin{bmatrix} \Delta\psi_{fd} \\ \Delta\psi_{fq} \end{bmatrix} \tag{A-14}$$

Eliminating $(\Delta i_d, \Delta i_q)$ and $(\Delta i_{fd}, \Delta i_{fq})$ from eqs. (A-5), (A-6) and (A-11)

$$\begin{bmatrix} \Delta E_q' \\ \Delta E_d' \end{bmatrix} = [X_{MF}][X_R]^{-1} \{[C_a] + [T_{fo}']p\}^{-1} [X_R][X_{MF}]^{-1} \left\{ \begin{bmatrix} \Delta E_{fd} \\ \Delta E_{fq} \end{bmatrix} - [X_s - X_s'][X_s' + X_e]^{-1} \begin{bmatrix} E\sin\delta_o \\ E\cos\delta_o \end{bmatrix} \Delta\delta \right\} \tag{A-15}$$

where $$[C_a] = [1] + [X_{MA}][X_s' + X_e]^{-1}[X_s - X_s'][X_{MA}]^{-1} \tag{A-16}$$

$$[T_{fo}'] = [X_R][R_F]^{-1} \tag{A-17}$$

$$\begin{bmatrix} \Delta E_{fd} \\ \Delta E_{fq} \end{bmatrix} = [X_{MF}][R_F]^{-1} \begin{bmatrix} \Delta e_{fd} \\ \Delta e_{fq} \end{bmatrix} \tag{A-18}$$

Equation (A-15) is expressed as follows.

$$\begin{bmatrix} \Delta E_q' \\ \Delta E_d' \end{bmatrix} = \{[C_A] + [T_{Fo}']p\}^{-1} \left\{ \begin{bmatrix} \Delta E_{fd} \\ \Delta E_{fq} \end{bmatrix} - [X_s - X_s'][X_s' + X_e] \begin{bmatrix} E\sin\delta_o \\ E\cos\delta_o \end{bmatrix} \Delta\delta \right\} \tag{A-19}$$

where $$\{[C_A] + [T_{Fo}']p\}^{-1} = [X_{MF}][X_R]^{-1}\{[C_a] + [T_{fo}']p\}^{-1}[X_R][X_{MF}]^{-1} \tag{A-20}$$

furthermore

$$\begin{bmatrix} \Delta E_q' \\ \Delta E_d' \end{bmatrix} = \{[1] + [T_{FZ}']p\}^{-1}[C_A]^{-1} \left\{ \begin{bmatrix} \Delta E_{fd} \\ \Delta E_{fq} \end{bmatrix} - [X_s - X_s'][X_s' + X_e] \begin{bmatrix} E\sin\delta_o \\ E\cos\delta_o \end{bmatrix} \Delta\delta \right\} \tag{A-21}$$

where $$[T_{FZ}'] = [C_A]^{-1}[T_{FO}'] \tag{A-22}$$

Substituting eqs. (A-3), (A-9) and (A-11) in eq. (A-1)

$$\Delta e_t = -[C_{eo}][X_s'][X_s' + X_e]^{-1} \begin{bmatrix} E\sin\delta_o \\ E\cos\delta_o \end{bmatrix} \Delta\delta + [C_{eo}][X_e][X_s' + X_e]^{-1} \begin{bmatrix} \Delta E_q' \\ \Delta E_d' \end{bmatrix} \tag{A-23}$$

Defining the following coefficients in eqs. (A-13), (A-21) and (A-23), eqs. (20), (21) and (22) in the text are obtained.

$$[K_1] = \{[\psi_o] - [I_o][X_s']\}[X_s' + X_e]^{-1} \begin{bmatrix} E\sin\delta_o \\ E\cos\delta_o \end{bmatrix} \tag{A-24}$$

$$[K_2] = \{[\psi_o] + [I_o][X_e]\}[X_s' + X_e]^{-1} \tag{A-25}$$

$$[K_3] = [C_A]^{-1} \tag{A-26}$$

$$[K_4] = [X_s - X_s'][X_s + X_e]^{-1} \begin{bmatrix} E\sin\delta_o \\ E\cos\delta_o \end{bmatrix} \tag{A-27}$$

$$[K_5] = -[C_{eo}][X_s'][X_s' + X_e]^{-1} \begin{bmatrix} E\sin\delta_o \\ E\cos\delta_o \end{bmatrix} \tag{A-28}$$

$$[K_6] = [C_{eo}][X_e][X_s' + X_e]^{-1} \tag{A-29}$$

NOMENCLATURE

D	damping torque coefficient. (p.u. torque/p.u. speed)
E	infinite bus voltage.
e_t	generator terminal voltage.
e_d, e_q	d-axis, q-axis components of generator terminal voltage.
e_{f1}, e_{f2}	f1, f2 winding field voltage.
e_{fd}, e_{fq}	d-axis, q-axis equivalent field voltage.
E_{fd}, E_{fq}	d-axis, q-axis equivalent field voltage converted into armature circuit.
E'_q, E'_d	d-axis, q-axis voltage proportional to equivalent field flux.
$G_{ar}(p)$	transfer function of angle regulator (AAR).
$G_{vr}(p)$	transfer function of voltage regulator (AVR).
i_d, i_q	d-axis, q-axis components of armature current.
i_{f1}, i_{f2}	f1, f2 winding field current.
i_{fd}, i_{fq}	d-axis, q-axis equivalent field current.
M	inertia constant.
p	differential operator d/dt.
T_e	electrical torque.
T_m	prim-mover torque.
T'_{fdo}, T'_{fqo}	d-axis, q-axis equivalent field winding open circuit time constant.
T'_{fdz}, T'_{fqz}	d-axis, q-axis equivalent field winding time constant on load.
$[X_e] = \begin{bmatrix} x_e & 0 \\ 0 & x_e \end{bmatrix}$	external reactance.
$[X_s] = \begin{bmatrix} x_d & 0 \\ 0 & x_q \end{bmatrix}$	synchronous reactance.
$[X_{mf}] = \begin{bmatrix} x_{a1}\cos\theta_1 & x_{a2}\cos\theta_2 \\ x_{a1}\sin\theta_1 & x_{a2}\sin\theta_2 \end{bmatrix}$	field winding magnetizing reactance.
$[X_{ma}] = \begin{bmatrix} x_{a1}\cos\theta_1 & x_{a1}\sin\theta_1 \\ x_{a2}\cos\theta_2 & x_{a2}\sin\theta_2 \end{bmatrix}$	field winding magnetizing reactance.
$[R_f] = \begin{bmatrix} r_{f1} & 0 \\ 0 & r_{f2} \end{bmatrix}$	field winding resistance.
$[X_r] = \begin{bmatrix} x_{ff1} & x_{f12} \\ x_{f21} & x_{ff2} \end{bmatrix}$	field winding reactance.
x_e	external reactance.
x_d, x_q	d-axis, q-axis synchronous reactance.
x'_d, x'_q	d-axis, q-axis transient reactance.
$x_{a1} = x_{ad}\cos^2\theta_1 + x_{aq}\sin^2\theta_1$	f1 winding magnetizing reactance.
$x_{a2} = x_{ad}\cos^2\theta_2 + x_{aq}\sin^2\theta_2$	f2 winding magnetizing reactance.
x_{ad}, x_{aq}	d-axis, q-axis magnetizing reactance.
r_{f1}, r_{f2}	f1, f2 winding resistance.
x_{ff1}, x_{ff2}	f1, f2 winding self reactance.
x_{f12}, x_{f21}	f1, f2 winding mutual reactance.
δ	rotor angle.
θ_1, θ_2	angle between f1 winding, f2 winding and the d-axis of the rotor.
ψ_d, ψ_q	d-axis, q-axis components of armature flux linkage.
ψ_{f1}, ψ_{f2}	f1, f2 winding field flux linkage.
ψ_{fd}, ψ_{fq}	d-axis, q-axis equivalent field flux linkage.
ω_o	base angular frequency.
ω	angular frequency of machine osillation.

Subscript 0 means steady state value.
Prefix Δ indicates small change.

REFERENCES

(1) R.G. Harley and B. Adkins, "Stability of synchronous machines with divided-winding rotor", Proc. IEE, Vol. 117, pp. 933-947, May, 1970.

(2) M. Rama Murthi, M. Williams and B.W. Hogg, "Stability of synchronous machine with 2-axis excitation systems", Proc. IEE, Vol. 117, pp. 1799-1808, September, 1970.

(3) Hamdi-Sepen, "Process for increasing the transient stability power limits on a.c. transmission systems", CIRGE, paper 305, 1962.

(4) D.P. Senqupta, B.W. Hogg and M. Yau, "Hunting characteristics of a synchronous machine with two field windings", Proc. IEE, Vol. 117, pp. 119-125, January, 1970.

(5) A.M. El-Serafi and M.A. Badr, "Analysis of the dual-excited synchronous machine", paper no. T 72 029-2, presented at IEEE Winter Meeting, New York, 1971.

(6) F.P. Demello and C. Concordia, "Concepts of Synchronous Machine Stability as Affected by Excitation Control", IEEE Transactions, PA&S, Vol. PAS-88, pp. 316-329, April, 1969.

CENTRAL SUPERVISION AND CONTROL OF THE POWER FLOW IN POWER SYSTEMS BY MEANS OF STEADY-STATE-SENSITIVITY ANALYSIS

Ch. Hendrich
Technical University
Munich, Germany

ABSTRACT

For central control of power flow in electric power systems the on-line-computer needs methods, which enable it to foresee and to compare in a very short time the effects of load-shedding or different active and reactive power injection on the steady-state of the system. For this purpose two methods have been tested with regard to accuracy and computation time. Methods and results are described in this report.

INTRODUCTION

An increase in security can be reached by means of central supervision and control of the power flow in electrical networks. In this way the uncontrolled switching off of lines by the noncentral overload protection and subsequent reactions can be avoided [1]. But to carry out this task, the computer needs a so called decision-help, which enables it to select the suitable measures in time, i.e. in about one minute, after getting the information that one or more branches are overloaded. Some of the most important measures are:

- Variation of the reactive load flow in the power system by changing the reactive power injection.
- Variation of the active power injection.
- Load-shedding

The question, which one of these measures is sufficient to reduce the overload of the branches, can only be answered by testing the effect of possible changes in the power injection or of load shedding.
For such sensitivity analysis the use of the Jacobian matrix is proposed [5]. This Newton's approximation method was the first one being tested for this special application. Then a Newton-Gauss approximation method was developed, which was as accurate as the Newton's method, and moreover it was faster, because the matrix to be solved was much smaller.

The consumer loads as a function of the voltage at these nodes were represented by using two different models. In the first model the consumer loads are represented by constant active and reactive power, i.e. the automatic regulation of the transformers is included. In the second model the loads are represented by constant active current and constant susceptance, i. e. the automatic regulation of the transformers is not included [2].

Notation

Matrices and vectors are enclosed in brackets and denoted by indices, which indicate the length of rows and columns; e.g. A_{NN}.
Complex numbers are denoted by a super bar; e.g. $\bar{U}$.

Index N : Number of all nodes in the network, without the slack-node.

Index G : Number of generation-nodes, without the slack-node.

Index L : Number of nodes, which are no generation nodes, here generally called consumer-nodes.

CONFERENCE PAPER

C 73 308-4. A paper recommended by the IEEE Power System Engineering Committee of the IEEE Power Engineering Society for presentation at the IEEE PES Summer Meeting & EHV/UHV Conference, Vancouver, Can., July 15-20, 1973. Manuscript submitted February 2, 1973; made available for printing April 17, 1973.

Price: Members $1.35
Nonmembers $1.80
At Meeting: $1.00

$\bar{v}_k = e_k + jf_k$; : complex node voltage at node k

v_k : node voltage magnitude

$[\bar{v}]_G$: complex voltage vector of the generation-nodes, without the slack-node

$[\bar{v}]_L$: complex voltage vector of the consumer-nodes

$P_k + jQ_k$: complex power into node k

$[\bar{I}]_L$: complex node current vector of the not - generation - nodes, i.e. consumer-nodes.

Always the first G nodes are generation-nodes, e.g.:

$$[\bar{Y}]_{NN} = \left[\begin{array}{c|c} [\bar{Y}]_{GG} & [\bar{Y}]_{GL} \\ \hline [\bar{Y}]_{LG} & [\bar{Y}]_{LL} \end{array}\right]_{NN}$$: Complex admittance matrix

Other symbols are explained as they appear in the text.

The Newton's approximation method

The Newton's method is generally known as a method with good and fast convergence [3,4]. It is logical to use the Jacobian matrix as a decision-help, as done in [5].

$$\left[\frac{[\Delta e]_N}{[\Delta f]_N}\right]_{2N} = [J]^{-1}_{2N\,2N} \cdot \left[\frac{[\Delta P]_N}{[\Delta F]_N}\right]_{2N} \qquad (1)$$

$[J]_{2N\ 2N}$ is the Jacobian matrix for the existing state of the power system.

$$[J]_{2N2N} = \left[\begin{array}{c|c} \frac{[\partial P]_N}{[\partial e]_N} & \frac{[\partial P]_N}{[\partial f]_N} \\ \hline \frac{[\partial F]_N}{[\partial e]_N} & \frac{[\partial F]_N}{[\partial f]_N} \end{array}\right]_{2N2N}$$

The expression F is representative for Q or v^2 as it is wanted. In general in the injection-nodes $F_k = v_k^2$ and $\Delta F_k = \Delta v_k^2 = 0$; and in the load nodes $F_i = Q_i$ and $\Delta F_i = \Delta Q_i$. Sometimes it may be more interesting to give a change of reactive power in some injection-nodes too, corresponding $F_k = Q_k$ and $\Delta F_k = \Delta Q_k$.

If the input is a possible change in the nodal complex power vector, $[\Delta P]_N + j[\Delta Q]_N$, it is possible to get immediately approximated values of the changes in the nodal voltage vector, $[\Delta e]_N + j[\Delta f]_N$ without iteration. With these voltages all interesting branch currents can be calculated.

The Newton-Gauss approximation method

By means of the normal admittance matrix $[\bar{Y}]_{N,N}$ it is possible to write the changes of the consumer voltages $[\Delta\bar{v}]_L$ as a function of the changes of consumer currents $[\Delta\bar{I}]_L$ and the changes of the generation voltages $[\Delta\bar{v}]_G$.

$$[\Delta\bar{v}]_L = [\bar{Y}]^{-1}_{LL} \cdot [\Delta\bar{i}]_L - [\bar{Y}]^{-1}_{LL} \cdot [\bar{Y}]_{LG} \cdot [\Delta\bar{v}]_G; \qquad (2)$$

The application of the Newton's method only to the generation-nodes yields (3):

$$\left[\frac{[\Delta P]_G}{[\Delta F]_G}\right]_{2G} = \left[\begin{array}{c|c} \frac{[\partial P]_G}{[\partial e]_G} & \frac{[\partial P]_G}{[\partial f]_G} \\ \hline \frac{[\partial F]_G}{[\partial e]_G} & \frac{[\partial F]_G}{[\partial f]_G} \end{array}\right]_{2G\,2G} \cdot \left[\frac{[\Delta e]_G}{[\Delta f]_G}\right]_{2G} + \left[\begin{array}{c|c} \frac{[\partial P]_G}{[\partial e]_L} & \frac{[\partial P]_G}{[\partial f]_L} \\ \hline \frac{[\partial F]_G}{[\partial e]_L} & \frac{[\partial F]_G}{[\partial f]_L} \end{array}\right]_{2G\,2L} \cdot \left[\frac{[\Delta e]_L}{[\Delta f]_L}\right]_{2L} \qquad (3)$$

where: $F_k = v_k^2$ or $F_k = Q_k$ respectively.

If only the power in generation-nodes is changed, the change of the consumer currents $[\Delta\bar{I}]_L$ is nearly zero.

$[\Delta\bar{I}]_L \approx 0$;

In this case eq. (3) together with eq. (2) can be written as follows:

$$\left[\frac{[\Delta e]_G}{[\Delta f]_G}\right]_{2G} = [C]^{-1}_{2G\,2G} \cdot \left[\frac{[\Delta P]_G}{[\Delta F]_G}\right]_{2G} \qquad (4)$$

where: